

Ultrahigh-energy Gamma-Ray Radiation from the Crab Pulsar Wind Nebula

LIN NIE,¹ YANG LIU,¹ ZEJUN JIANG,¹ AND XIONGFEI GENG²

¹*Department of Astronomy, Yunnan University, and Key Laboratory of Astroparticle Physics of Yunnan Province, Kunming, 650091, People's Republic of China.*

²*School of Electrical and Information Technology, Yunnan Minzu University, Kunming 650091, Yunnan, People's Republic of China.*

ABSTRACT

It has been long debated whether the high-energy gamma-ray radiation from the Crab nebula stems from leptonic or hadronic processes. In this work, we investigate the multiband nonthermal radiation from the Crab pulsar wind nebula with the leptonic and leptonic–hadronic hybrid models, respectively. Then we use the Markov Chain Monte Carlo sampling technology and method of sampling trace to study the stability and reasonability of the model parameters according to the recently observed results and obtain the best-fitting values of parameters. Finally, we calculate different radiative components generated by the electrons and protons in the Crab nebula. The modeling results indicate that the pure leptonic origin model with the one-zone only can partly agree with some segments of the data from various experiments (including the PeV gamma-ray emission reported by the LHAASO and the other radiation ranging from the radio to very-high-energy gamma-ray wave band), and the contribution of hadronic interaction is hardly constrained. However, we find that the hadronic process may also contribute, especially in the energy range exceeding the PeV. In addition, it can be inferred that the higher energy signals from the Crab nebula could be observed in the future.

Keywords: Gamma-rays(637); Radiative process(2055); Rotation powered pulsars(1408); Nebulae(1095)

1. INTRODUCTION

It is believed that pulsar wind nebulae (PWNe) are an important high-energy radiative sources in the Galaxy. The PWNe are also known as candidates for Galactic cosmic ray sources. It is suggested that the PWNe inside supernova remnants (SNRs) can further accelerate the relativistic protons accelerated by the SNR shock to the energy of PeV (Ohira et al. 2018). Therefore, as a PeVatron, the PWNe will accelerate the charged particles (electrons and protons) to relativistic energy and produce the multiband nonthermal photons with energies ranging from radio to ultra-high-energy gamma-ray bands.

The Crab Nebula is one of the comprehensively studied celestial objects, and is an important cosmic laboratory for exploration of the nonthermal relativistic processes in astrophysical settings (Aharonian & Atoyan 1995). It has an age of ~ 940 yr, lies at a distance of $d \sim 2$ kpc, and is powered by the pulsar PSR J0534+2200 which has a rotational period of 33.4 ms and a period derivative of $4.23 \times 10^{-13} \text{ s s}^{-1}$ (Lyne et al. 1993). It has been observed in radio (Baars & Hartsuijker 1972), FIR (Bandiera et al. 2002), optical (Veron-Cetty & Woltjer 1993), soft X-rays, gamma rays, and very-high-energy gamma rays (Albert et al. 2008; Aharonian et al. 2021; Kuiper et al. 2001; Amenomori et al. 2019).

Table 1. The best-fitting parameters for the leptonic model.

Model	α_1	α_2	η	$B_{PWN}(uG)$	$E_{cut}(TeV)$	$\varepsilon_0(TeV)$
leptonic	$1.533^{+0.0056}_{-0.0065}$	$2.51^{+0.0031}_{-0.0033}$	$0.265^{+0.0034}_{-0.0032}$	$129.42^{+1.8}_{-1.78}$	$0.154^{+0.0059}_{-0.0061}$	$5.649^{+0.052}_{-0.051} \times 10^3$

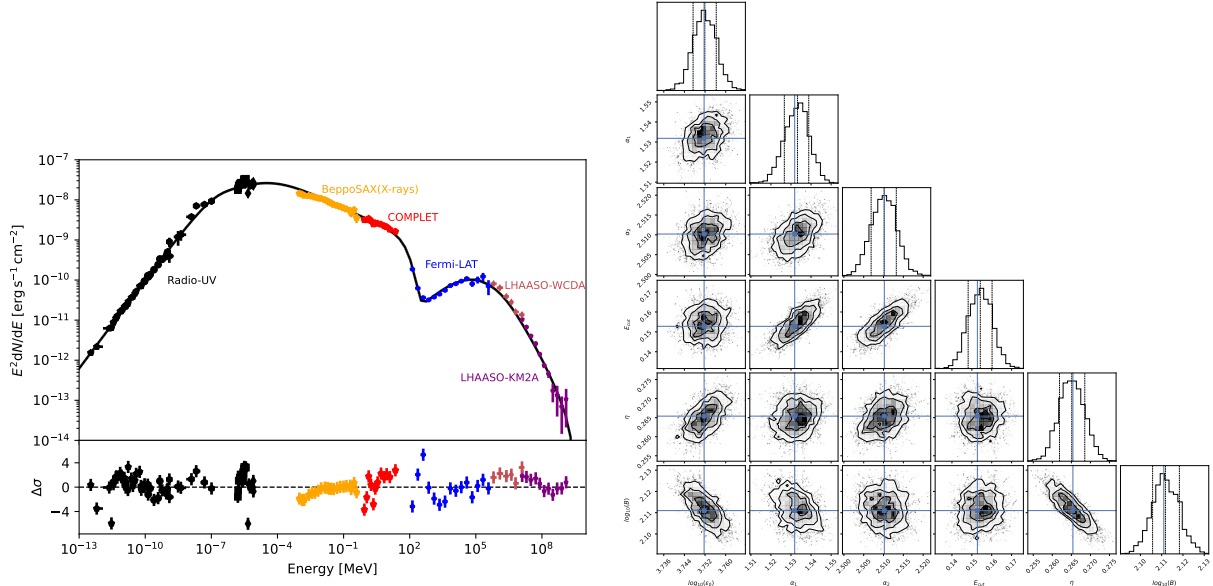


Figure 1. The right panel shows the distribution of the model parameters for the one-zone leptonic model, the parameter vector with the highest likelihood found during the run is indicated by the blue cross. The left panel presents the spectrum of the Crab Nebula, which includes the modeling spectrum from the leptonic model, multiwave band observational data, and the residual of the maximum likelihood model (bottom panel in the left panel plot). The thick black line indicates the maximum likelihood spectrum, and the gray lines present samplings of the posterior distribution of the model parameter vector. The observational data with energy ranging from the radio to UV come from Baars & Hartsuijker (1972), Bandiera et al. (2002), and Veron-Cetty & Woltjer (1993), the X-ray and MeV data of COMPTTEL take from the Kuiper et al. (2001), the blue data come from the observation of Fermi Large Area Telescope (Arakawa et al. 2020), the firebrick and purple data points have been reported by (Cao et al. 2021a).

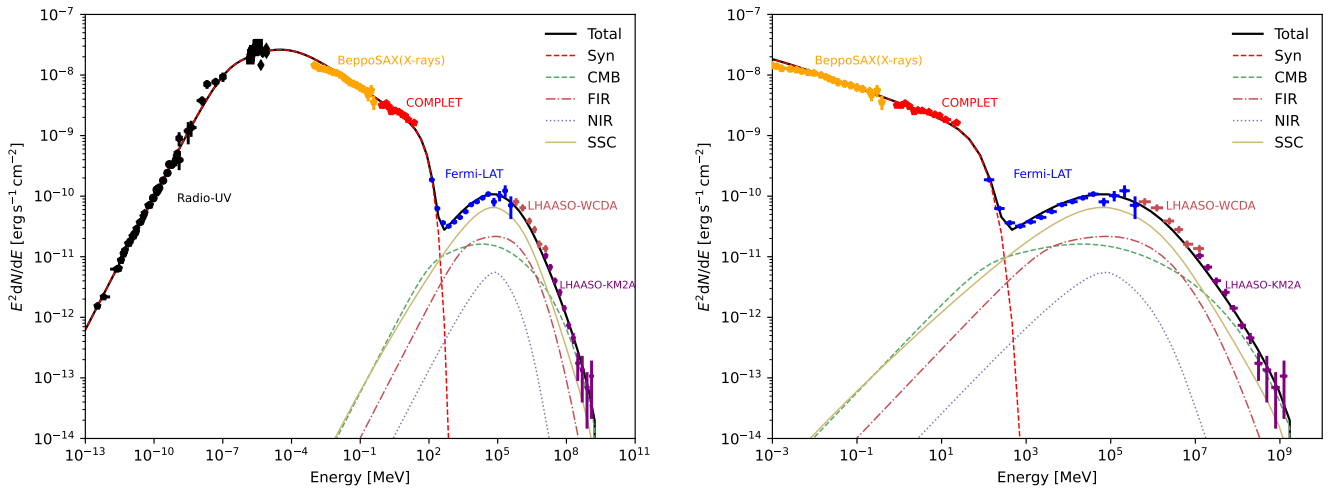


Figure 2. The Crab nebula SEDs were calculated with the leptonic model. The left panel is a multiwave band nonthermal spectrum and the right panel shows that with energy ranging from X-ray to ultra-high-energy bands. The black solid line is the total spectrum, the red dashed line presents the synchrotron emission, and the IC scatterings with the synchrotron photons (yellow solid line), FIR (dash-dotted line), CMB (green dashed line), and NIR (dotted line) are shown. The same as Fig.1 for the observed data.

It is generally thought that the emission from radio to medium energy gamma rays is generated by the injected electrons through the synchrotron radiative mechanism. The high-energy photon emission mainly comes from Inverse Compton (IC) scattering of the high-energy electrons on the background seed photons, which include the synchrotron

background, the cosmic microwave background, and infrared photons in the PWNe (see, e.g., Zhang et al. 2008; Fang & Zhang 2010; Torres et al. 2013; Lu et al. 2020). On the other hand, it is also suggested that the gamma rays could be emitted by the hadronic processes. The relativistic protons accelerated in the Crab pulsar outer gap interact with the matter inside the nebula, and this process may contribute in the high-energy gamma-ray range (see, e.g., Cheng et al. 1990; Bednarek & Protheroe 1997; Khangulyan et al. 2020; Cao et al. 2021a). Therefore, it has been long debated whether the high-energy emission from the PWNe is the leptonic or hadronic origin. The details of the high-energy radiation produced by leptonic process have been discussed for the Crab nebula (see, e.g., Venter & de Jager 2007; Zhang et al. 2008; Martín et al. 2012), and that of the gamma-ray emission about the hadronic process have been also investigated (see, e.g., Cheng et al. 1990; Bednarek & Protheroe 1997; Bednarek 2003, 2007). However, with the establishment of more and more high-energy observatories, some telescopes have possessed the performance of observing photons of exceeding to the PeV from the astronomic objects. An increasing number of observational data has been reported by the different experiments. For example, the Amenomori et al. (2019) reported that the Tibet air shower array with the underground water-Cerenkov-type muon detector array observed the highest energy photons of exceeding 100 TeV with a 5.6σ statistical significance and pointed the measured spectrum with energy extended to the sub-PeV from the Crab nebula have an absence of high-energy cutoff. Recently, more than 530 photons at energies above 100 TeV and up to 1.4 PeV from the 12 ultra-high-energy gamma-ray sources with a statistical significance greater than seven standard deviations were reported again by LHAASO (Cao et al. 2021b). Together with the earlier investigations about the leptonic scenario, the radiative spectrum from the leptons has a cutoff around the sub-PeV region (see, e.g., Zhang et al. 2008; Martín et al. 2012; Zhang et al. 2020). It seems that the other components of gamma rays have a significant contribution.

In this paper, we investigated multiband nonthermal radiation from the Crab pulsar wind nebula with the leptonic and leptonic–hadronic hybrid model, respectively. We simulated the broadband nonthermal radiation which includes components of leptonic and hadronic origin. In addition, we derived the best-fitting values and distribution of the model parameters with the method of the Markov Chain Monte Carlo (MCMC) sampling to analyze the reasonability and stability of fitting parameters in the physics and to further constrain the parameters of the model base on the recently observed data.

2. MODEL AND RESULT

2.1. Leptonic Origin Model

In this model, the pulsar associated with the PWN loses its rotational energy via a pulsar wind composed of magnetic and high-energy particles to power the high-energy physical process inside the nebula (Atoyan & Aharonian 1996; Fang & Zhang 2010). The relativistic wind of particles driven by the pulsar is blown into the ambient medium and generates a termination shock wave, which accelerates the electrons to relativistic energy. These relativistic electrons interact with the magnetic field and low-energy background photons (the synchrotron, thermal, FIR, and microwave background radiation), and generate the multiband nonthermal photons with energies ranging from radio to high-energy gamma-ray bands (Zhang et al. 2008; Fang & Zhang 2010; Lu et al. 2017). According to the review of the leptonic model (see, e.g., Zhang et al. 2008; Venter & de Jager 2007; Torres et al. 2013), the electrons injected into PWNe are accelerated by the pulsar magnetosphere and the termination shock. Therefore, the relativistic particles injected into the PWNe are also assumed as two different power-law components from the pulsar magnetosphere and shock acceleration, respectively. The injected spectrum of relativistic electrons inside PWNe is described as

$$Q(E_e, t) = \begin{cases} Q_0(t)(E_e/E_{\text{cut}})^{-\alpha_1} & \text{if } E_e < E_{\text{cut}} \\ Q_0(t)(E_e/E_{\text{cut}})^{-\alpha_2} & \text{if } E_e \geq E_{\text{cut}} \end{cases} \quad (1)$$

where the Q_0 can be determined by the $\int Q(E_e, t)E_e dE_e = \eta L(t)$; η is the conversion efficiency from spin-down power into electron luminosity. The maximum energy of the electrons was express as $E_{max}(t) \approx \varepsilon_0 \sqrt{\frac{L(t)}{L_0}}$, and L_0 is initial spin-down power. The electron energy distribution was given by

$$\frac{dN(E_e, T_{age})}{dt} = \int_0^{T_{age}} Q(E_e, t) \exp\left(-\frac{T_{age} - t}{\tau_{eff}}\right) dt \quad (2)$$

where the $\tau_{eff}^{-1} = \tau_{esc}(t)^{-1} + \tau_{syn}(t)^{-1}$, $\tau_{esc}(t)$ is the escape timescale, and $\tau_{syn}(t)$ is the lifetime of the relativistic electron of the synchrotron emission loss. The details of temporal evolution about the electron in the PWNe are discussed by the Zhang et al. (2008)(also see the version of Fang & Zhang 2010; Lu et al. 2017).

After the electron distribution is determined, we calculate multiband nonthermal radiation via the mechanism of the synchrotron radiation and IC scattering. For the calculation of the synchrotron radiation and IC scattering, we use the formalism of Blumenthal & Gould (1970).

In this model, we consider $\alpha_1, \alpha_2, \varepsilon_0, E_{cut}, \eta$, and B_{PWB} as the free parameters that determine the distribution of the injected electrons and the radiative spectra. In the calculative process, we use the MCMC sampling method to derive the best-fitting values of model parameters and the distribution of the free parameters. We obtained the values of parameters and show them in Table.1. In Fig.1 and Fig.2, we show modeling results that include the distribution of parameters, and results of comparison between the theoretical spectrum with the best-fitting model parameters and observed data. Furthermore, we used the *plot_chain* function of *Naima* (Zabalza 2015) to plot the diagnostic figure of sampling about the fitting parameters to judge whether the sampling has stabilized around the maximum likelihood parameters, and the results of the sampling are presented in Fig.6 (see the Appendix.A). Besides, the bottom left of each panel in Fig.6 (see the Appendix.A) provides statistics of parameter distribution with the medium value, which has uncertainties based on the 16th and 84th percentiles.

Finally, we use this model with best-fitting parameters to compute the total energy of electrons in Crab nebula $W_e \approx 7.299_{-0.0044}^{+0.0046} \times 10^{48}$ erg.

As shown in Fig.1, some data have a strong signal of deviation from the model. In the range from 1 MeV to 500 MeV, the COMPTEL data seem off from the model, with at least 6σ , and Fermi data in this range are off by at least 10σ , with a totally different trend. In the VHE energy range between 1 and ~ 100 TeV, the observed data is lower than the prediction by 4σ . On the other hand, the observational data have a steeper spectrum than the model predictions between ~ 50 and ~ 500 TeV, while that around PeV have an opposite trend. Importantly, for the PeV photons, the acceleration rate of parent electrons at the site of PeV photons was described as (Cao et al. 2021a) $\eta = 0.14(B/100\mu G)(E_\gamma/1PeV)^{1.54}$. We obtained magnetic field strength of $B \sim 130$ uG through fitting multiband data with the one-zone leptonic model. This means that the acceleration rate of the parent electron is larger than 21% for the photons with energies up to 1.1 PeV. This scenario is inconsistent with the magnetohydrodynamic (MHD; the acceleration rate of the electron in the young supernova remnants is smaller by exceeding 3 orders of magnitude; Malkov & Drury 2001; Cao et al. 2021a). Therefore, it is perhaps necessary to introduce a new component to explain the PeV radiation from the Crab nebula.

2.2. Leptonic-Hadronic Origin Model

For the hadronic process, it is thought that the neutron star atmosphere consists mainly of irons (Venkatesan et al. 1997). The Fe nuclei of the neutron star surface can escape from the polar cap surface of the pulsar and move along magnetic field lines to enter the pulsar magnetosphere where those heavy nuclei can be accelerated by the potential (Cheng et al. 1990; Bednarek & Protheroe 1997). After the acceleration of the pulsar magnetosphere, the partial particles will escape from the pulsar magnetosphere along the open magnetic field lines and be injected into the PWN. During the propagation process, the Fe nuclei and the other heavy nuclei will interact with the background photons and suffer disintegration in the collisions with soft photons produced inside the pulsar outer gap. The injected rate of Fe nuclei was given as (Bednarek & Protheroe 1997)

$$\dot{N}_{Fe} = \xi L_{Crab}(B, P)/Z\Phi(B, P) \quad (3)$$

where ξ is the fraction of the total power taken by relativistic nuclei accelerated in the outer gap; Z is the atomic number of Fe. And the potential difference across the outer gap can be described simply as $\Phi(B, P) \approx 5 \times 10^{16}(B/4 \times 10^{12}G)(P/s)^{4/3}$ V, B is the surface magnetic field of the pulsar.

The protons emitted directly in the disintegration process and those protons from neutron decay in the evolution process are captured by the nebula and accumulated in the PWNe. Therefore, the proton spectrum was described as

$$\frac{dN_p}{dE} = \left[\frac{dN_p(\gamma_p, t_{CN})}{dE} \right]_1 + \left[\frac{dN_p(\gamma_p, t_{CN})}{dE} \right]_2 \quad (4)$$

Here, the proton spectrum from the neutron decaying is (Bednarek & Protheroe 1997)

$$\begin{aligned} \left[\frac{dN_p(\gamma_p, t_{CN})}{dE} \right]_1 &= \gamma_p^{-1} \int_0^{t_{CN}} dt \dot{N}_{Fe}(t) e^{-\tau_{nH}(t)} \\ &\times \left[N_n(\gamma_p(t), t) \gamma_p(t) [1 - \exp(-vt/c\gamma_p(t)\tau_n)] + \right. \\ &\left. \int_t^{t_{CN}} dt' N_n(\gamma_p(t'), t) \gamma_p(t') \frac{\exp(-vt'/c\gamma_p(t')\tau_n)}{c\gamma_p(t')\tau_n} \right] \end{aligned} \quad (5)$$

and the direct proton spectrum derived from the photodisintegration of the Fe nuclei and the other heavy nuclei is (Yang & Zhang 2009)

$$\begin{aligned} \left[\frac{dN_p(\gamma_p, t_{CN})}{dE} \right]_2 &= \frac{\gamma_p(t)}{\gamma_p} \dot{N}_{Fe}(t) \frac{dt}{dP} \frac{dP}{dE_p(t)} \\ &e^{-\tau_{nH}(t)} \int_0^{\gamma_p(t)} d\gamma' N_p(\gamma') \end{aligned} \quad (6)$$

where number of the i nucleons at energy E_i ($i = n, p$) per unit energy per one nucleus was approximated $N_{n,p}(E_{n,p}) \approx \frac{Al_{gap}R_{A,i}}{Z\Phi(B,P)c}$, the l_{gap} is the dimension of the outer gap, $R_{A,i}$ is the photodisintegration rate of nuclei. Its calculative detail in the PWNe was described in Bednarek & Protheroe (1997). Here A is atomic number of nucleus and $\gamma_p(t)$ presents the Lorentz factor at time t . The $\tau_{nH}(t)$ and τ_n present the optical depth and neutron decaying time, respectively. In the calculated process, we adopt the $\xi = 0.85$ fitted in Bednarek (2003).

The protons provided in the above are accelerated by the pulsar magnetosphere. However, the emission with energy extended to the PeV has been observed through the LHAASO (Cao et al. 2021b) and this indicates that the primary particles need to reach the energy of exceeding PeV. But the iron nuclei accelerated in the inner magnetosphere or the Crab pulsar wind zone may mainly contribute in the TeV gamma-ray range (Cheng et al. 1990; Bednarek 2003). In this paper, we assume an extra component of the proton spectrum as the exponential cutoff power-law distribution

$$\frac{dN}{dE} = A_p E_p^{-\alpha_p} \exp\left(-\frac{E}{E_{p,c}}\right) \quad (7)$$

Here, A_p is the normalization factor. We constrain the parameter A_p with the observed data in the sub-PeV to PeV energy range. The $E_{p,c}$ is cutoff energy of protons. According to the discussion in some literature, the protons can be accelerated up to an energy above 30 PeV (Blasi et al. 2000; Zhang et al. 2020; Bucciantini et al. 2011). Some acceleration sites in the Crab nebula may provide a source of ultrarelativistic light protons with an injection spectrum, steepening to E^{-2} at higher energies (Arons 2003). Here, we fix the index $\alpha_p = 2.0$ and set $E_{p,c} = 30$ PeV due to constraint with few PeV data. We adopt a mean gas density, which is estimated as $n_H \sim 10 \text{ cm}^{-3}$ for the Crab nebula with the radius $R_{pwn} = 1.8$ pc (Zhang et al. 2020; Cao et al. 2021a).

In order to explain the multiwavelength observational results from the PWNe, the contribution provided by the leptons is essential. The electrons generate photons through synchrotron, bremsstrahlung, and IC scattering mechanisms; and protons produce the gamma rays via the decay of π^0 mesons in proton–proton interactions. Here, based on the distribution of electrons and protons, we calculated the multiband nonthermal emission. The gamma-ray radiation from proton–proton interaction is calculated using the expressions of Kelner et al. (2006) and the bremsstrahlung is calculated via the formalism of Blumenthal & Gould (1970).

However, the model assumes that the emission is produced in an idealized one-zone bulk in Section 2.1. This estimate is based on the assumption that the magnetic field has a uniform distribution or is slowly varying. Furthermore, the numerical results of PWNe have shown clearly that the distribution of the magnetic field and the maximum energy of the emitting particles can change quite dramatically within the nebula (Volpi et al. 2008). The MeV synchrotron radiation and sub-PeV IC emission are mainly produced by the electron population with energy exceeding ~ 450 TeV (see, e.g., Khangulyan et al. 2020; Cao et al. 2021a). On the other hand, the structure that the gamma-ray spectrum in the 1 – 100 MeV band is not smooth can be reproduced by the electron population with an exponential cutoff $E_{cut} \sim 450$ TeV and a hard energy distribution peaking at higher energies (Khangulyan et al. 2020). Therefore, we set the electron population to have an exponential cutoff energy $E_0 = 450$ TeV, assuming the MeV synchrotron radiation

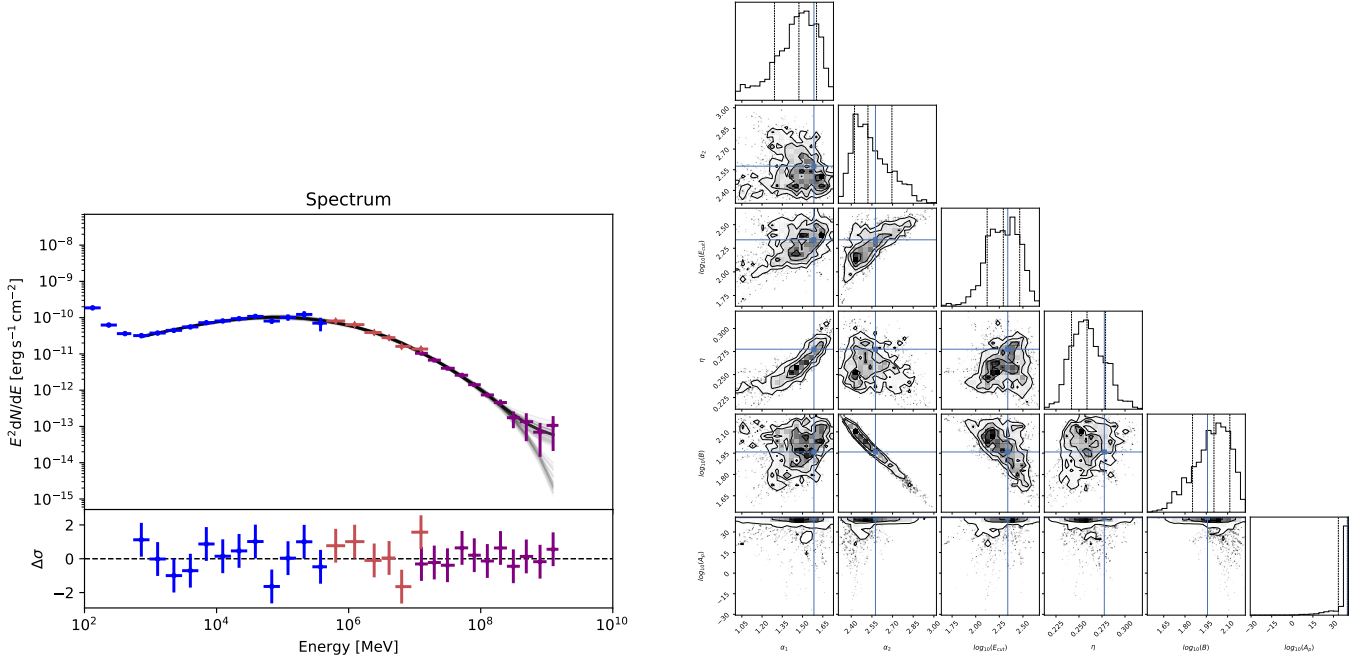


Figure 3. The same as Fig.1 but the hadronic and bremsstrahlung components have been considered. This hybrid model adds a free parameters (A_p) and ignores the parameter ϵ_0 due to setting the exponential cutoff energy of electrons to $E_0 = 450$ TeV.

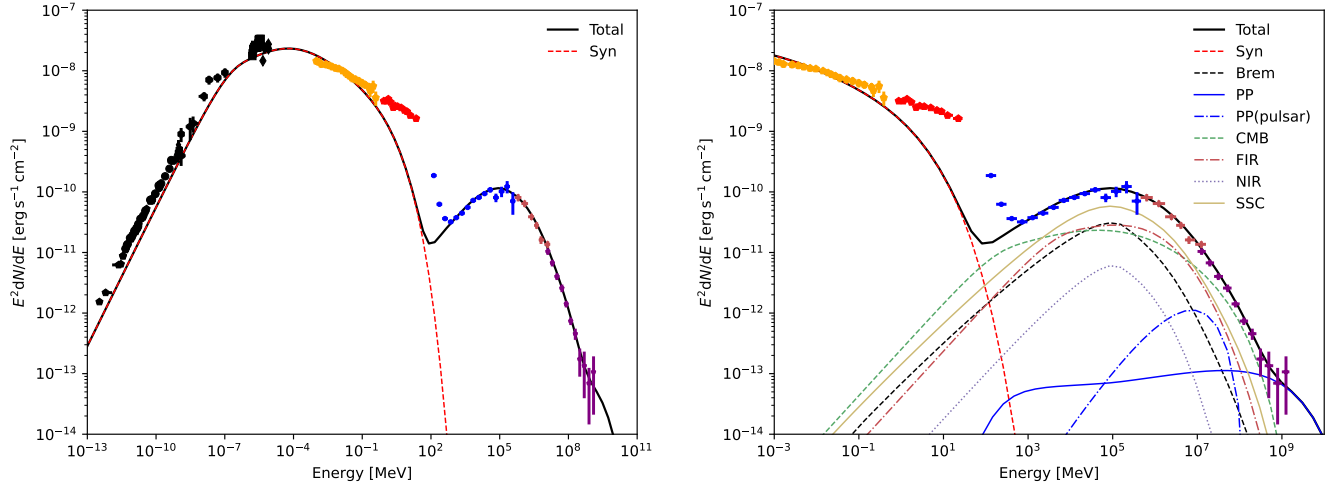


Figure 4. The same as Fig.2 but the hadronic and bremsstrahlung components have been considered. Here, the blue dashed-dotted line presents the component of protons that originates from the photodisintegration of Fe in the pulsar magnetosphere; the blue solid line is an extra component from the protons. The black dashed line shows the bremsstrahlung of electrons.

and PeV IC emission have different origins. Then we use the new component from the proton to provide the extra PeV emission. We mainly focus on the high-energy emission, namely the GeV to PeV emission. Here, the data with energy below GeV, which may have a more complicated origin, is ignored during the fitting process.

It is similar to the treatment method of the one-zone leptonic model in Section 2.1. Together with the leptonic scenario introduced in Section 2.1, we refit the observed data ranging from GeV to PeV gammarays for the Crab nebula with the MCMC approach. As results of the analysis, we show statistics of the parameter distribution, which includes a medium with uncertainties based on the 16th and 84th percentiles in Fig.7 (see the Appendix.A). we also show the corner plot, which plots the distribution for all parameters against each other and the spectral energy

Table 2. The best-fitting parameters for the leptonic–hadronic model.

Model	α_1	α_2	η	$B_{\text{PWN}}(uG)$	$E_{\text{cut}}(\text{TeV})$	$A_p(eV^{-1})$
leptonic–hadronic	$1.49^{+0.13}_{-0.18}$	$2.53^{+0.13}_{-0.09}$	$0.259^{+0.02}_{-0.015}$	$102.33^{+23.56}_{-6.83}$	$0.204^{+0.071}_{-0.075}$	$1.58^{+1.57}_{-1.56} \times 10^{40}$

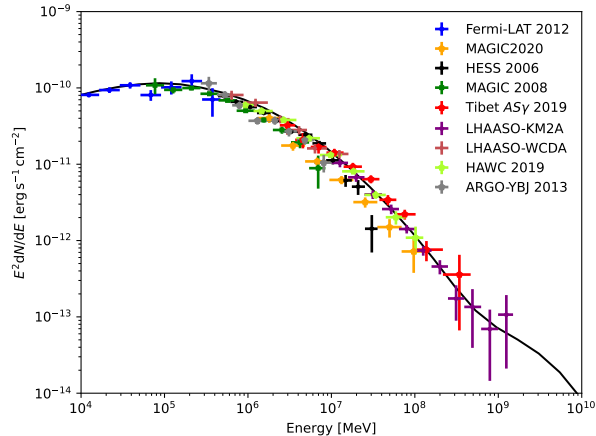


Figure 5. Gamma-ray spectrum of the Crab Nebula. The gamma-ray data are taken from the High-Energy Stereoscopic system (H.E.S.S.; Aharonian et al. (2006)), the Major Atmospheric Gamma Imaging Cerenkov (MAGIC) telescopes (MAGIC Collaboration et al. 2020), the High Altitude Water Cherenkov (HAWC) Gamma-ray Observatory (Abeysekara et al. 2019), the Fermi Large Area Telescope (Arakawa et al. 2020), Astrophysical Radiation by Ground-based Observation at Yang Ba Jing (Bartoli et al. 2015), Tibet AS γ (Amenomori et al. 2019), and LHAASO (Cao et al. 2021a). The black solid line is the same as the one in the left panel of Fig.3.

distribution with the best-fitting parameters in Fig.3 and Fig.4. The results present that this electron population underestimates the fluxes in the radio to ultraviolet (UV) bands. This is in favor of the scenario that the radio–UV emission has a more complicated mechanism, which is consistent with the previous investigation (Lyutikov et al. 2019). But the data and model have a smaller deviation in the energy range above GeV, compared with the one-zone leptonic situation in Section 2.1. And the data can be described better.

As a result of the calculation, the best-fitting parameters of the leptonic–hadronic model are listed in Table.2. The fitting values of some parameters that have been fitted with the MCMC in Section 2.1 have a significant change. Finally, we obtain the total energy in protons inside the Crab nebula $W_p = 3.64^{+4.08}_{-3.6} \times 10^{47}$ erg.

3. CONCLUSION AND DISCUSSION

The nonthermal emission from the Crab nebula, with the energy ranging from radio to high-energy gamma ray bands, is emitted by the injected electrons through synchrotron emission and IC scattering mechanism, or is also produced via the decay of π^0 mesons in the proton–proton interaction process. Based on the previous investigation, the observational data ranging from radio to high-energy gamma rays reported by the different observatories is generally interpreted as a strong argument in favor of a leptonic origin (see, e.g., Martín et al. 2012; Torres et al. 2013; Zhu et al. 2015). On the other hand, the hadronic origin is also naturally used to account for the high-energy gamma-ray emission (see, e.g., Bednarek & Protheroe 1997; Bednarek 2003). Therefore, it is argued that it is difficult to distinguish the leptonic and hadronic origin of the emission with energy exceeding ~ 10 TeV for the Crab nebula (see, e.g., Bednarek 2003; Yang & Zhang 2009; Khangulyan et al. 2020; Zhang et al. 2020).

In order to calculate the multiwave band nonthermal radiation from the PWNe, we need to determine the basic parameters of pulsar and nebula. For the Crab nebula, the break index $n = 2.5$, initial period $P_0 = 19$ ms and moment of inertia $I = 1.0 \times 10^{45}$ g cm² have been known (Bednarek 2003, 2007; Zhang et al. 2008). In this paper, we model the multiwavelength nonthermal radiation from the Crab nebula with the leptonic origin model and leptonic–hadronic hybrid model, respectively. In addition, we use the method of Markov Chain Monte Carlo sampling to obtain the value of the maximum likelihood parameters and their uncertainties.

We find out that the leptonic model with the one-zone fails to describe the broadband observed data in detail, and the hadronic component may be crucial for gamma-ray emission from the Crab nebula. This is because, in some energy range, the emission may have a different origin. For instance, the ~ 100 keV – MeV emission may arise from a superposition of two components (Lyutikov et al. 2019). With the report of gamma-ray flares (100 MeV – 10 GeV) from the Crab nebula (Mayer et al. 2013; Arakawa et al. 2020), it is thought that the MeV radiation might be produced in a special region with special physical conditions (e.g. the particles are accelerated by the magnetic reconnection or a small-scale magnetic turbulence is present) which are different from the typical conditions expected in the Crab nebula (Cerutti et al. 2012; Kelner et al. 2013; Luo et al. 2020). The radio to UV emission is the most complicated and its resulting broadband SEDs include synchrotron emission of the accumulated long-living leptons, thermal emission from the dust in the nebula, and optical line emission from the filaments (Meyer et al. 2010). Therefore, when we fit the global data within the one-zone leptonic model, the constraint to the model is mathematically suppressed and some segments of data show a strong signal of deviation from the model. For the VHE gamma-ray emission, although we cannot distinguish whether it is dominated by the leptonic or hadronic origin, it is responsible to constrain some parameters together with the contribution provided by the hadronic interaction process.

On the other hand, the gamma-ray emission beyond PeV could need an extra radiative component. This is because, although the spectrum simulated via the one-zone leptonic model seems to explain the observational PeV data (see Fig.1), the observational data of around 1.1 PeV with the highest energy reported by the LHAASO (Cao et al. 2021a) have a higher flux than that of the prediction. Importantly, the acceleration rate of emitting electrons at such high energy is higher than 21%. This could be a huge challenge to the ideal MHD or even classical electrodynamics. While the leptonic–hadronic scenario perhaps is a reasonable result. It has a smaller deviation (see Fig.4). In addition, the PeV emission was also explained as an extra exponent from leptons, which originates from regions with $B < 100$ uG (Cao et al. 2021a). But it remains to be explored whether the PeV photons are dominated by the electrons and we leave it to future studies.

We show the previous measurements in Fig.5. They are almost consistent with the model and the observation of LHAASO. Yet there seems to be a deviation from the model for the measurement of different experiments. The data of HAWC and Tibet AS γ have a smaller deviation that is consistent with the WCDA and KM2A data. While the data from H.E.S.S, MAGIC, and ARGO-YBJ are lower than the prediction of the model. This could be due to the experiments with different systematic uncertainty.

In the fitting process of the leptonic–hadronic hybrid model, base on the constraint of the current data ranging from GeV to ultra-high-energy gamma-rays which have been reported, we calculate the energy of exceeding PeV in protons as $W_{p,>PeV} \sim 5.95^{+7.16}_{-5.89} \times 10^{46}$ erg inside the Crab nebula. We find that the contribution of hadronic interaction is hardly constrained. It should be remarked that the parameter (A_p) is not stabilized very well in the fitting process (see Fig.7) due to few observational data with energy extended to the PeV. It is mainly constrained by the gamma-ray data of extending PeV. Therefore, it needs further observation to provide constraints or evidence for the contribution of hadronic interaction in the future.

ACKNOWLEDGEMENTS

We thank the referee for providing some suggestions. This work is partially supported by the National Key Research and Development Program 2018YFA0404204, the National Natural Science Foundation of China (NSFC U1931113, U1738211), and the Foundations of Yunnan Province (2018FY001(-003)).

APPENDIX

A. THE STABILITY OF MODEL PARAMETERS AROUND THE BEST-FITTING VALUES

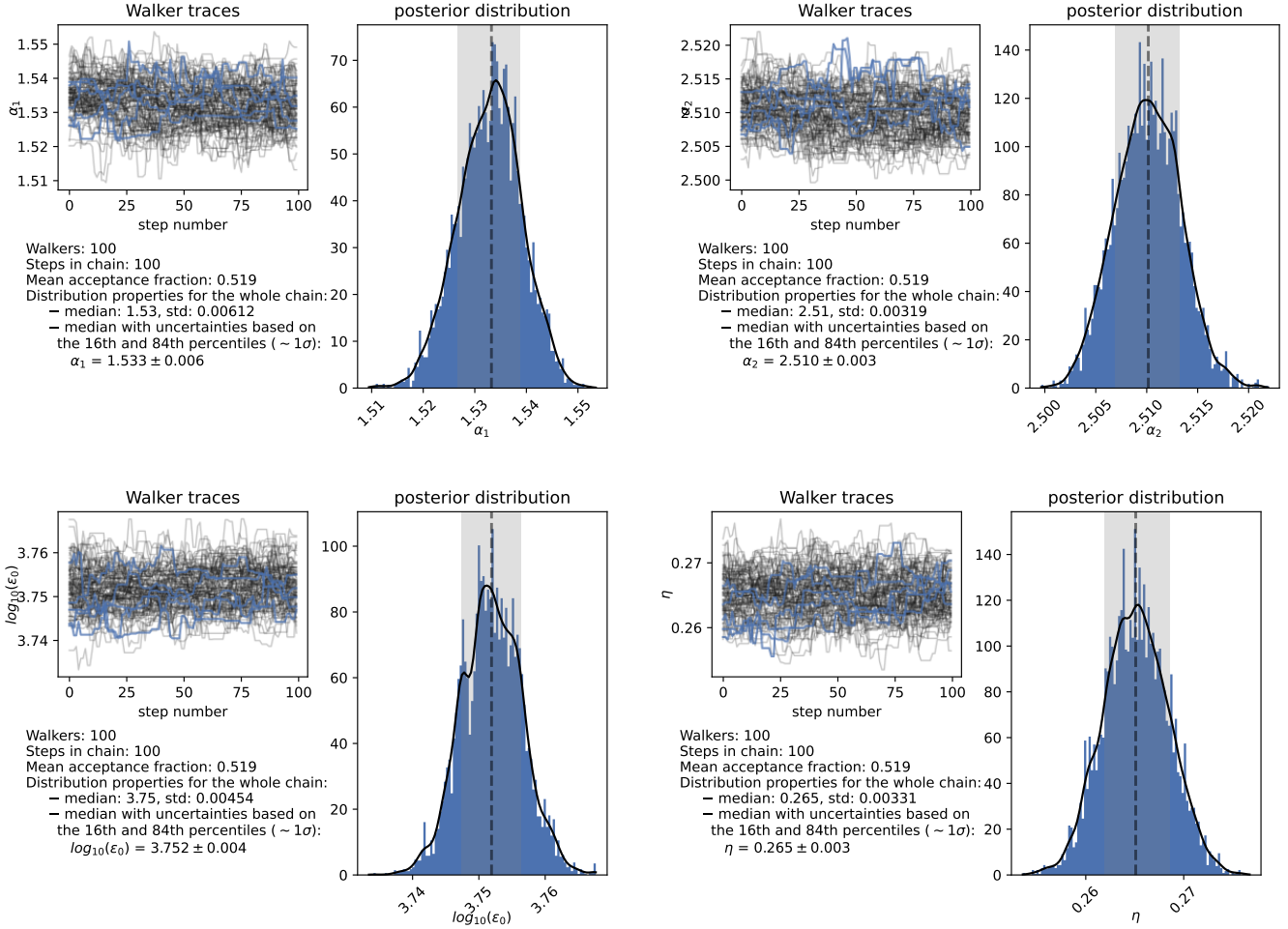


Figure 6. The diagnostic figure in the sampling of the parameters in the leptonic model. The top-left panel shows the traces for the 100 workers in gray and three of them are highlighted in blue in each panel, which can be used to estimate whether the sampling has stabilized around the maximum likelihood parameters. The right panel shows the posterior distribution of the parameters in the individual plot. (Figure 6 continued on next page)

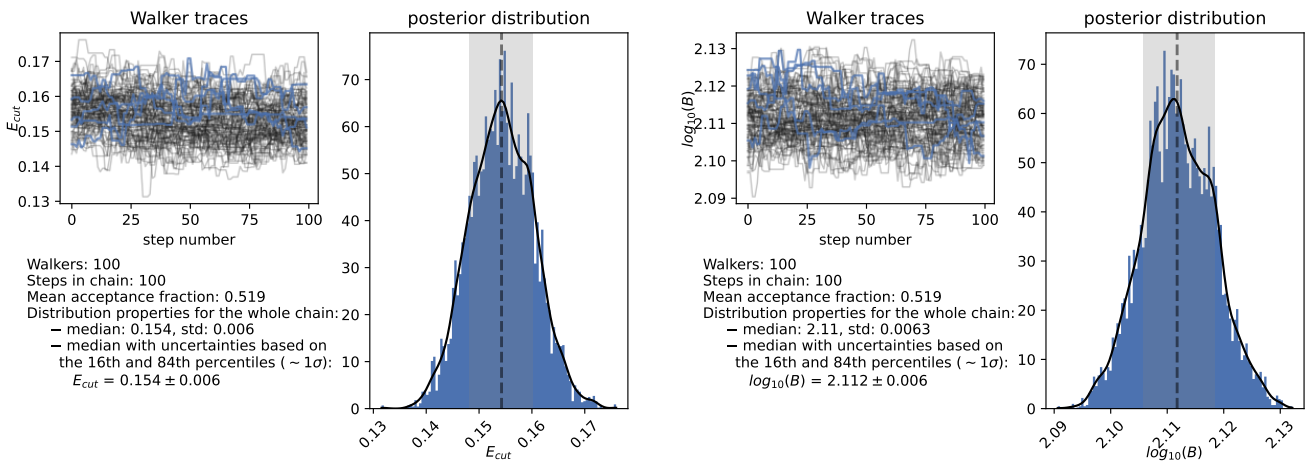


Figure 6. (continued)

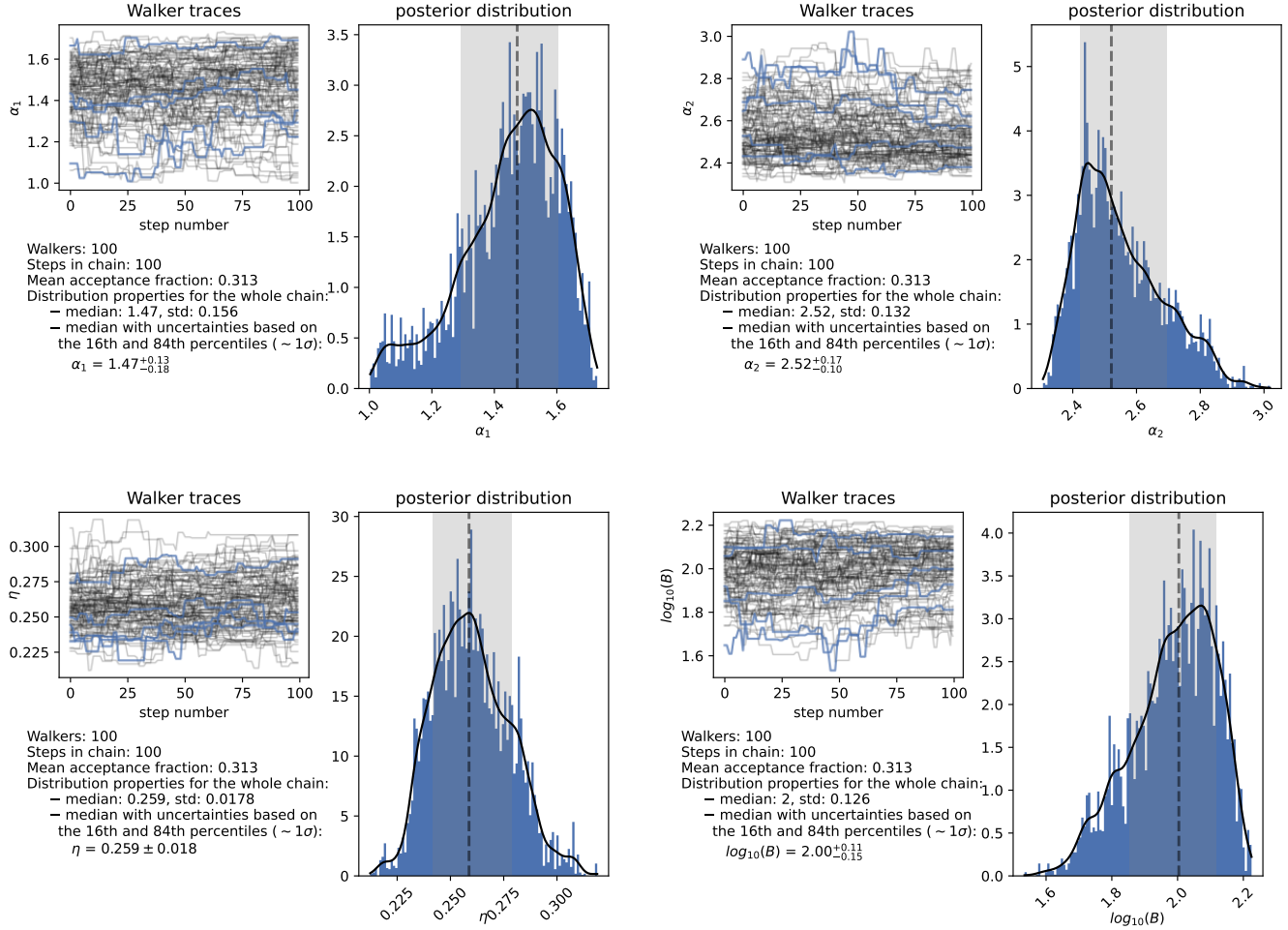


Figure 7. The same as Fig.6 but for the leptonic–hadronic hybrid model.

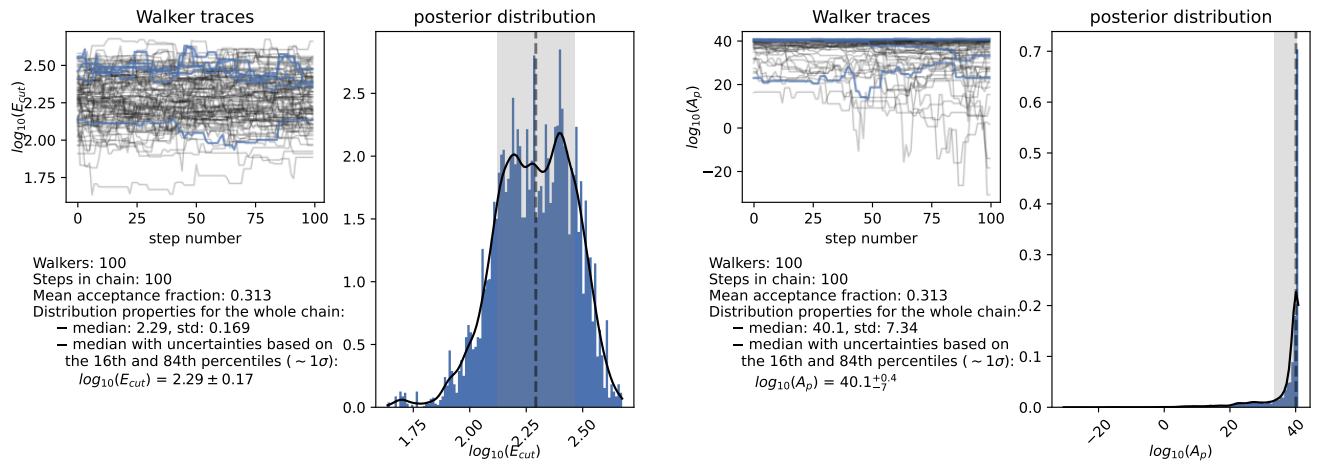


Figure 7. (continued)

REFERENCES

- Abeyssekara, A. U., Albert, A., Alfaro, R., et al. 2019, *ApJ*, 881, 134, doi: [10.3847/1538-4357/ab2f7d](https://doi.org/10.3847/1538-4357/ab2f7d)
- Aharonian, F., Akhperjanian, A. G., Bazer-Bachi, A. R., et al. 2006, *A&A*, 457, 899, doi: [10.1051/0004-6361:20065351](https://doi.org/10.1051/0004-6361:20065351)
- Aharonian, F., An, Q., Axikegu, et al. 2021, *Chinese Physics C*, 45, 025002, doi: [10.1088/1674-1137/abd01b](https://doi.org/10.1088/1674-1137/abd01b)
- Aharonian, F. A., & Atoyan, A. M. 1995, *Astroparticle Physics*, 3, 275, doi: [10.1016/0927-6505\(95\)00006-3](https://doi.org/10.1016/0927-6505(95)00006-3)
- Albert, J., Aliu, E., Anderhub, H., et al. 2008, *ApJ*, 674, 1037, doi: [10.1086/525270](https://doi.org/10.1086/525270)
- Amenomori, M., Bao, Y. W., Bi, X. J., et al. 2019, *PhRvL*, 123, 051101, doi: [10.1103/PhysRevLett.123.051101](https://doi.org/10.1103/PhysRevLett.123.051101)
- Arakawa, M., Hayashida, M., Khangulyan, D., & Uchiyama, Y. 2020, *ApJ*, 897, 33, doi: [10.3847/1538-4357/ab9368](https://doi.org/10.3847/1538-4357/ab9368)
- Arons, J. 2003, *ApJ*, 589, 871, doi: [10.1086/374776](https://doi.org/10.1086/374776)
- Atoyan, A. M., & Aharonian, F. A. 1996, *MNRAS*, 278, 525, doi: [10.1093/mnras/278.2.525](https://doi.org/10.1093/mnras/278.2.525)
- Baars, J. W. M., & Hartsuiker, A. P. 1972, *A&A*, 17, 172
- Bandiera, R., Neri, R., & Cesaroni, R. 2002, *A&A*, 386, 1044, doi: [10.1051/0004-6361:20020325](https://doi.org/10.1051/0004-6361:20020325)
- Bartoli, B., Bernardini, P., Bi, X. J., et al. 2015, *ApJ*, 798, 119, doi: [10.1088/0004-637X/798/2/119](https://doi.org/10.1088/0004-637X/798/2/119)
- Bednarek, W. 2003, *A&A*, 407, 1, doi: [10.1051/0004-6361:20030929](https://doi.org/10.1051/0004-6361:20030929)
- . 2007, *Ap&SS*, 309, 179, doi: [10.1007/s10509-007-9396-9](https://doi.org/10.1007/s10509-007-9396-9)
- Bednarek, W., & Protheroe, R. J. 1997, *PhRvL*, 79, 2616, doi: [10.1103/PhysRevLett.79.2616](https://doi.org/10.1103/PhysRevLett.79.2616)
- Blasi, P., Epstein, R. I., & Olinto, A. V. 2000, *ApJL*, 533, L123, doi: [10.1086/312626](https://doi.org/10.1086/312626)
- Blumenthal, G. R., & Gould, R. J. 1970, *Reviews of Modern Physics*, 42, 237, doi: [10.1103/RevModPhys.42.237](https://doi.org/10.1103/RevModPhys.42.237)
- Bucciantini, N., Arons, J., & Amato, E. 2011, *MNRAS*, 410, 381, doi: [10.1111/j.1365-2966.2010.17449.x](https://doi.org/10.1111/j.1365-2966.2010.17449.x)
- Cao, Z., Aharonian, F., An, Q., et al. 2021a, *Science*, 373, 425, doi: [10.1126/science.abg5137](https://doi.org/10.1126/science.abg5137)
- Cao, Z., Aharonian, F. A., An, Q., et al. 2021b, *Nature*, 594, 33, doi: [10.1038/s41586-021-03498-z](https://doi.org/10.1038/s41586-021-03498-z)
- Cerutti, B., Werner, G. R., Uzdensky, D. A., & Begelman, M. C. 2012, *ApJL*, 754, L33, doi: [10.1088/2041-8205/754/2/L33](https://doi.org/10.1088/2041-8205/754/2/L33)
- Cheng, K. S., Cheung, T., Lau, M. M., Yu, K. N., & Kwok, P. W. 1990, *Journal of Physics G Nuclear Physics*, 16, 1115, doi: [10.1088/0954-3899/16/7/022](https://doi.org/10.1088/0954-3899/16/7/022)
- Fang, J., & Zhang, L. 2010, *A&A*, 515, A20, doi: [10.1051/0004-6361/200913615](https://doi.org/10.1051/0004-6361/200913615)
- Kelner, S. R., Aharonian, F. A., & Bugayov, V. V. 2006, *PhRvD*, 74, 034018, doi: [10.1103/PhysRevD.74.034018](https://doi.org/10.1103/PhysRevD.74.034018)
- Kelner, S. R., Aharonian, F. A., & Khangulyan, D. 2013, *ApJ*, 774, 61, doi: [10.1088/0004-637X/774/1/61](https://doi.org/10.1088/0004-637X/774/1/61)
- Khangulyan, D., Arakawa, M., & Aharonian, F. 2020, *MNRAS*, 491, 3217, doi: [10.1093/mnras/stz3261](https://doi.org/10.1093/mnras/stz3261)
- Kuiper, L., Hermsen, W., Cusumano, G., et al. 2001, *A&A*, 378, 918, doi: [10.1051/0004-6361:20011256](https://doi.org/10.1051/0004-6361:20011256)
- Lu, F.-W., Gao, Q.-G., & Zhang, L. 2017, *ApJ*, 834, 43, doi: [10.3847/1538-4357/834/1/43](https://doi.org/10.3847/1538-4357/834/1/43)
- . 2020, *MNRAS*, 498, 1911, doi: [10.1093/mnras/staa2338](https://doi.org/10.1093/mnras/staa2338)
- Luo, Y., Lyutikov, M., Temim, T., & Comisso, L. 2020, *ApJ*, 896, 147, doi: [10.3847/1538-4357/ab93c0](https://doi.org/10.3847/1538-4357/ab93c0)
- Lyne, A. G., Pritchard, R. S., & Graham Smith, F. 1993, *MNRAS*, 265, 1003, doi: [10.1093/mnras/265.4.1003](https://doi.org/10.1093/mnras/265.4.1003)
- Lyutikov, M., Temim, T., Komissarov, S., et al. 2019, *MNRAS*, 489, 2403, doi: [10.1093/mnras/stz2023](https://doi.org/10.1093/mnras/stz2023)
- MAGIC Collaboration, Acciari, V. A., Ansoldi, S., et al. 2020, *A&A*, 635, A158, doi: [10.1051/0004-6361/201936899](https://doi.org/10.1051/0004-6361/201936899)
- Malkov, M. A., & Drury, L. O. 2001, *Reports on Progress in Physics*, 64, 429, doi: [10.1088/0034-4885/64/4/201](https://doi.org/10.1088/0034-4885/64/4/201)
- Martín, J., Torres, D. F., & Rea, N. 2012, *MNRAS*, 427, 415, doi: [10.1111/j.1365-2966.2012.22014.x](https://doi.org/10.1111/j.1365-2966.2012.22014.x)
- Mayer, M., Buehler, R., Hays, E., et al. 2013, *ApJL*, 775, L37, doi: [10.1088/2041-8205/775/2/L37](https://doi.org/10.1088/2041-8205/775/2/L37)
- Meyer, M., Horns, D., & Zechlin, H. S. 2010, *A&A*, 523, A2, doi: [10.1051/0004-6361/201014108](https://doi.org/10.1051/0004-6361/201014108)
- Ohira, Y., Kisaka, S., & Yamazaki, R. 2018, *MNRAS*, 478, 926, doi: [10.1093/mnras/sty1159](https://doi.org/10.1093/mnras/sty1159)
- Torres, D. F., Cillis, A. N., & Martín Rodríguez, J. 2013, *ApJL*, 763, L4, doi: [10.1088/2041-8205/763/1/L4](https://doi.org/10.1088/2041-8205/763/1/L4)
- Venkatesan, A., Coleman Miller, M., & Olinto, A. V. 1997, *ApJ*, 484, 323, doi: [10.1086/304304](https://doi.org/10.1086/304304)
- Venter, C., & de Jager, O. C. 2007, in *WE-Heraeus Seminar on Neutron Stars and Pulsars 40 years after the Discovery*, ed. W. Becker & H. H. Huang, 40. <https://arxiv.org/abs/astro-ph/0612652>
- Veron-Cetty, M. P., & Woltjer, L. 1993, *A&A*, 270, 370
- Volpi, D., Del Zanna, L., Amato, E., & Bucciantini, N. 2008, *A&A*, 485, 337, doi: [10.1051/0004-6361:200809424](https://doi.org/10.1051/0004-6361:200809424)
- Yang, X. C., & Zhang, L. 2009, *A&A*, 496, 751, doi: [10.1051/0004-6361/200810871](https://doi.org/10.1051/0004-6361/200810871)
- Zabalza, V. 2015, in *International Cosmic Ray Conference*, Vol. 34, 34th International Cosmic Ray Conference (ICRC2015), 922. <https://arxiv.org/abs/1509.03319>
- Zhang, L., Chen, S. B., & Fang, J. 2008, *ApJ*, 676, 1210, doi: [10.1086/527466](https://doi.org/10.1086/527466)
- Zhang, X., Chen, Y., Huang, J., & Chen, D. 2020, *MNRAS*, 497, 3477, doi: [10.1093/mnras/staa2151](https://doi.org/10.1093/mnras/staa2151)

Zhu, B.-T., Fang, J., & Zhang, L. 2015, MNRAS, 451, 3145,
doi: [10.1093/mnras/stv1140](https://doi.org/10.1093/mnras/stv1140)